Sense and Avoid for Unmanned Aircraft Systems: Ensuring Integrity and Continuity for Three Dimensional Intruder Trajectories

Michael B. Jamoom*, Mathieu Joerger† and Boris Pervan‡
Illinois Institute of Technology, Chicago, IL, 60616, USA

***Abstract*—This research aims at developing methods to meet safety targets for sense and avoid (SAA) sensors of Unmanned Aircraft Systems (UAS) through integrity and continuity risk evaluation. The SAA problem is presented as a three-dimensional, two-body problem. A Kalman filter approach is introduced to accommodate arbitrary sensor suites. Aircraft relative position and velocity estimates, referred to as *trajectory state* estimates, are transformed into *hazard state* estimates, which are used to quantify integrity and continuity risks. A sensitivity analysis is performed based on a set of representative, near-worst-case, three-dimensional intruder trajectories. The resulting impact on integrity and continuity is quantified for a composite nominal sensor. The concepts and methods in this research are intended to be used as a tool for certification authorities to set potential requirements for integration into the national airspace system.**

INTRODUCTION

The Need for Sense and Avoid

In the last two decades, unmanned aircraft systems (UAS) operated on a limited basis in the National Airspace System (NAS) supporting mostly public functions [1]. However, UAS operations are rapidly encompassing more civil and commercial applications [1]. With increased interest, the United States Congress mandated the Federal Aviation Administration (FAA), through the *FAA Modernization and Reform Act of 2012*, to develop requirements necessary for broader UAS access into the NAS [2]. To meet this mandate, the FAA must ensure an acceptable level of safety. To do this, a UAS requires a "sense and avoid" (SAA) capability to provide self-separation and collision avoidance (CA) protection between the UAS and other aircraft analogous to the "see and avoid" responsibility for pilots of manned aircraft [1].

Depending on the airspace classification, if an intruder aircraft is cooperative, that is, employing an operating transponder or Automatic Dependent Surveillance - Broadcast (ADS-B) [3], air traffic control (ATC) may provide separation. Alternatively, a manned aircraft pilot could employ a Traffic Collision Avoidance System (TCAS) as a situational awareness aid to help the pilot detect the intruder then initiate an avoidance maneuver. Otherwise, if the intruder aircraft is non-cooperative, without an operating transponder or ADS-B, the manned aircraft pilot will not have the help of ATC or TCAS. In this manned aircraft case, it is solely the pilot's responsibility to visually see the intruder and maneuver to maintain separation. Since UAS will not have a pilot on board, it will have to replicate the functionality of pilot vision through an appropriate sensor. Detection of non-cooperative aircraft will require, for example, an electro-optical (EO), infrared (IR) or radar sensor. This sensor must adequately inform the UAS SAA system whether or not a separation maneuver is required.

Self-Separation and Collision Avoidance

Although self-separation is a widely recognized term by the FAA and International Civil Aviation Organization (ICAO), it has never been fully cod-

*PhD Candidate, Department of Mechanical, Materials and Aerospace Engineering
†Research Assistant Professor, Department of Mechanical, Materials and Aerospace Engineering
‡Professor, Department of Mechanical, Materials and Aerospace Engineering

ified [4]. "Well clear" is a subjective term in the right-of-way rules, 14 CFR 91.113 [5], [6]. In 2011, Weibel, et al., proposed well clear as an objective separation standard [7]. In 2013, the Second FAA SAA Workshop concluded that the concept of well clear is an airborne separation standard [4]. Also in 2013, Lee, et al., demonstrated a capability, using the NASA Airspace Concept Evaluation System (ACES) model, to determine the rate of well clear violations for various well clear definitions [8]. In August 2014, the RTCA Special Committee-228 (SC-228) Sense and Avoid Science and Research Panel (SARP) defined well clear as having a horizontal time to closest point of approach (CPA), τ, of 35 seconds, a horizontal miss distance of 4000 feet and a vertical miss distance of 700 feet [9].

When an intruder cannot remain well clear, a CA maneuver is required to avoid a near mid-air collision (NMAC). NMAC boundaries are typically 500 feet laterally and 100 feet vertically from the own aircraft [4]. If the intruder aircraft is non-cooperative, it is up to the UAS SAA system to provide the appropriate CA maneuver.

Figure 1 depicts the conceptual difference between the WCT and NMAC distance thresholds (not to scale and not accounting for τ). For simplicity, we will concentrate on self-separation and WCT. The methodology is the same for CA and NMAC.

Problem Statement and Prior Work

SAA safety targets need to be met. This requires methods to quantify safety performance as a function of sensor uncertainty. In [10], the authors introduced and provided methods to evaluate *integrity risk* and *continuity risk* as UAS SAA safety performance metrics. These methods can be used to establish sensor performance requirements and can apply to any candidate sensor or sensor suite. In this paper, we refine that work to accommodate three dimensional intruder trajectories, which is challenging because (a) the geometry of an intruder penetrating the WCT cylinder from any direction must be properly captured, and (b) the integrity and continuity risks vary over time as the intruder approaches and additional sensor data are processed.

There have been several papers that provide overviews of the SAA problem. In 2000, Kuchar and Yang outlined an overview of air traffic conflict detection and resolution models [11]. In 2004, Drumm, et al., reviewed the problem in terms of "remotely piloted vehicles in civil airspace" [12]. In 2008, Dalamagkidis, et al., outlined UAS issues, challenges and restrictions for NAS integration [13]. In 2012, Prats, et al., looked at requirements, challenges and issues for UAS SAA [14]. Finally, in 2015, Yu and Zhang presented the current scope of the entire SAA problem, describing current SAA sensors, decision algorithms, path planning, and path following with a journal literature review [15].

Previous work has tended to focus on mirroring safety studies applicable to the ubiquitous TCAS. McLaughlin and Zeitlin described a MITRE safety study that used encounter models to build collision avoidance risk ratios to determine the safety of TCAS version 6.4 [16]. Espindle, et al., described an MIT Lincoln Lab safety study that used encounter models to build collision avoidance risk ratios to determine the safety of TCAS version 7.1 [17]. The Second SAA Workshop determined, using methodology described in the International Civil Aviation Organization (ICAO) Doc 9689, that UAS SAA systems should have two target levels of safety (TLS) based on catastrophic collision risk ratios: 10^{-9} midair collisions (MAC) per flight hour (FH) for cooperative airspace (where transponders are required) and 10^{-7} MAC/FH for all other airspace [4], [18]. Kim, et al., designed a 3D EO system for small UASs using a Kalman filter, Sequential Quadratic Programming, and Linear Parameter Varying approaches for tracking and measurement error reduction [19]. Kochenderfer, et al., developed an aircraft encounter model used to evaluate safety of CA systems using NMAC rate and risk ratio, which is defined as the NMAC rate with the CA system divided by the NMAC rate without the CA system [20]. Kochenderfer, Chryssanthacopoulos, and Billingsley looked at state uncertainty of a collision avoidance system, quantifying safety as probability of NMAC accounting for avoidance maneuvers, and applying Markov decision processes for CA [21], [22]. Heisley, et al., developed an architecture with a future intent to test and certify SAA systems

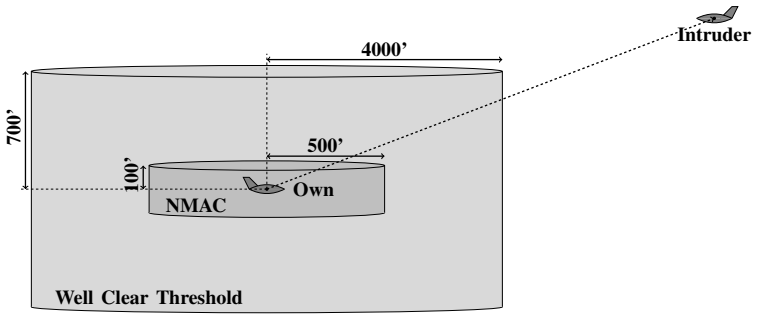

Fig. 1. Well Clear Threshold and Near Mid-Air Collision Distances (Not to Scale)

[23]. Lee, et al., constructed a distributed traffic model to enable a probabilistic approach to risk assessment by computing collision rates based on Predator training missions in the Grand Forks Air Force Base area [24]. Owen, et al., demonstrated and flight tested an approach to developing SAA radar models for requirements derivations that employed a phased-array technology [25]. Edwards and Owen validated a radar-based SAA concept through modeling and flight test [26].

Our approach is different, focusing directly on the accepted aviation navigation certification standards that quantify integrity and continuity as safety factors [27]. For example, for the Local Area Augmentation System (LAAS), at near-zero visibility, navigation integrity requirements specify that no more than one undetected hazardous navigation system failure is allowed in a billion approaches [28]. Kelly and Davis broke down their proposed TLS for required navigation performance (RNP) into accuracy, integrity, and continuity requirements [29], which are three of the four parameters that quantify navigation system performance (the other being availability) [29], [30]. This research focuses on integrity and continuity because they are the most difficult requirements for avionics systems to achieve.

Contributions of This Work

The SAA system needs to initiate a self-separation maneuver early enough to ensure the intruder aircraft remains outside the WCT. The horizontal tau self-separation threshold, τ_{SS}, represents the minimum time required to initiate the self-separation maneuver to prevent a WCT violation. Spatially, the intruder trajectory must be within both the WCT horizontal and vertical miss distances (MD), r_{MD} and z_{MD}, to be considered a hazard.

The method established in this work provides the means to set requirements on SAA sensors to ensure APV safety during three-dimensional encounters with intruder aircraft. This analysis identifies trade-offs between sensor characteristics and airspace capacity while maintaining integrity and continuity requirements.

Paper Outline

After this introductory section, the second section introduces the estimation model. The middle sections review the prior work methodology implementing SAA integrity and continuity. The section after that includes a sensitivity analysis depicting three dimensional intruder trajectories. The final section provides conclusions.

RELATIVE INTRUDER STATE ESTIMATION

We present the SAA problem as a three dimensional, two-body problem. The two bodies are the own aircraft and the intruder aircraft. The coordinate frame will always be an own-aircraft-centered body frame. Figure 2 is a graphical depiction of the own aircraft and the intruder aircraft in the horizontal and vertical planes. In the horizontal plane, we orient the x and y axes such that the x-axis is directly out of the nose of the own aircraft.

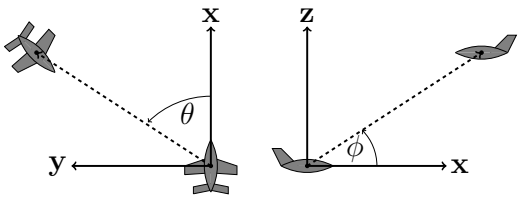

Fig. 2. Horizontal and Vertical Position of the Intruder Aircraft

The azimuth, θ, is the angle counterclockwise from the x-axis to the horizontal range vector (from the origin to the intruder position on the xy-plane). The elevation, ϕ, is the angle from the xy-plane up to the slant range vector (from the origin to the intruder position on the xz-plane). A particular sensor may measure the intruder's relative position (with error) in spherical, Cartesian, or cylindrical coordinates. In this development, we assume measurement vectors and measurement error covariance matrices are converted to Cartesian coordinates for processing.

Measurement Model

The own aircraft makes a measurement, $\mathbf{z}_n$, at time t_n of the intruder position, $\left[\begin{array}{ccc} x_n & y_n & z_n \end{array}\right]^T$:

$$\mathbf{z}_n = \mathbf{H}\mathbf{x}_n + \mathbf{v}_n \qquad \mathbf{v}_n \sim N(\mathbf{0}, \mathbf{V}_n) \tag{1}$$

The constant observation matrix $\mathbf{H}$ is:

$$\mathbf{H} = \left[\begin{array}{cc} \mathbf{I}_{3\times3} & \mathbf{0}_{3\times3} \end{array}\right] \tag{2}$$

The trajectory state vector, $\mathbf{x}_n$, is time variant, based on current intruder position and velocity:

$$\mathbf{x}_n = \left[\begin{array}{cccccc} x_n & y_n & z_n & \dot{x}_n & \dot{y}_n & \dot{z}_n \end{array}\right]^T \tag{3}$$

$N(\mathbf{a}, \mathbf{B})$ represents a normal distribution with mean, $\mathbf{a}$, and covariance, $\mathbf{B}$. $\mathbf{v}_n$ is the t_n measurement error, which we assume is over-bounded in the cumulative distribution function (CDF) sense by a Gaussian function with covariance matrix $\mathbf{V}_n$ [31], [32]. We also assume that a sample interval, Δt, is selected large enough to ensure independence of sequential sensor measurement errors.

The discrete-time process-noise-free state-transition equation is:

$$\mathbf{x}_n = \mathbf{\Phi}\mathbf{x}_{(n-1)} \tag{4}$$

where Φ represents the constant state-transition matrix for a constant relative velocity encounter.

$$\mathbf{\Phi} = \left[\begin{array}{cc} \mathbf{I}_{3\times3} & \Delta t\mathbf{I}_{3\times3} \\ \mathbf{0}_{3\times3} & \mathbf{I}_{3\times3} \end{array}\right] \tag{5}$$

Kalman Filter Implementation

This subsection presents a Kalman filter implementation to get the trajectory state estimate error covariance matrix. A Kalman filter approach is more computationally efficient than the batch estimator implemented in prior work [10]. It also allows for easy integration of different types of sensors. The following equations show how we implement the measurement and state transition equations, (1) and (4), in a Kalman filter. [33], [34].

We assume no prior knowledge on the trajectory states. The state estimate prediction is:

$$\bar{\mathbf{x}}_n = \mathbf{\Phi}\hat{\mathbf{x}}_{(n-1)} \tag{6}$$

and the estimate error prediction covariance:

$$\bar{\mathbf{P}}_n = \mathbf{\Phi}\hat{\mathbf{P}}_{(n-1)}\mathbf{\Phi}^T \tag{7}$$

The state estimate update is:

$$\hat{\mathbf{x}}_n = \bar{\mathbf{x}}_n + \mathbf{K}_n(\mathbf{z}_n - \mathbf{H}\bar{\mathbf{x}}_n) \tag{8}$$

and the estimate error covariance is:

$$\hat{\mathbf{P}}_n = (\mathbf{I} - \mathbf{K}_n\mathbf{H})\bar{\mathbf{P}}_n \tag{9}$$

where the Kalman gain matrix is:

$$\mathbf{K}_n = \bar{\mathbf{P}}_n\mathbf{H}^T(\mathbf{H}\bar{\mathbf{P}}_n\mathbf{H}^T + \mathbf{V}_n)^{-1} \tag{10}$$

The 6×6 trajectory state covariance matrix, $\hat{\mathbf{P}}$, is used to determine hazard state variances in the next section.

HAZARD STATES

For two-dimensional horizontal trajectories, the hazard states that describe a potential hazard with an intruder aircraft are the horizontal time to CPA, τ, and horizontal distance from the own aircraft to CPA, r_{CPA}. The left part of figure 3 is an overhead depiction of the horizontal CPA. For a WCT violation, the intruder must be within the WCT. That means r_{CPA} is smaller than or equal to the horizontal miss distance (MD), r_{MD}.

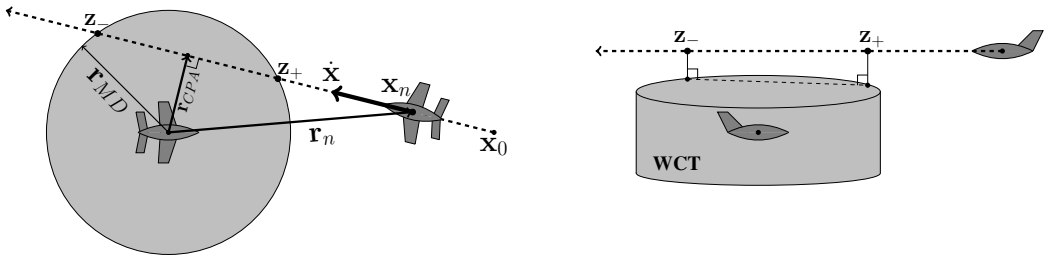

Fig. 3. Overhead and Side View of Hazard States

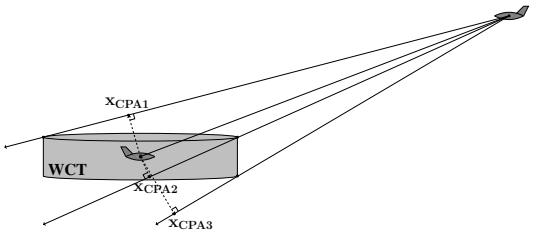

Fig. 4. Head-on Trajectories with 3D Closest Points of Approach

For a 3D WCT, there are some trajectories where either the vertical distance at the 3D CPA or the vertical distance at the 2D horizontal CPA are outside the WCT distance cylinder, but the intruder still penetrates the WCT distance cylinder. For example, consider the head-on trajectories depicted in Figure 4. Because the WCT distance thresholds define a cylinder and not a sphere, the trajectory intercepting the WCT at the top-back has a 3D CPA, labeled x_{CPA1}, which is outside the WCT occurring prior to WCT entry. Also, the trajectory that intercepts the bottom-front edge of the WCT has a 3D CPA, labeled x_{CPA3}, which is outside the WCT occurring after WCT entry.

To account for this, we add two vertical hazard states, z_+ and z_-, depicted in figure 3. Given that the intruder trajectory penetrates the horizontal WCT circle, z_+ is the vertical distance when the intruder trajectory enters the 2D horizontal WCT circle and z_- is the vertical distance when the intruder trajectory exits the 2D horizontal WCT circle. Note if $r_{CPA} = r_{MD}$ then $z_+ = z_-$.

Hazard State Equations

True τ (time to horizontal CPA) in terms of the trajectory states is:

$$\tau_n = \frac{-(\dot{x}_n x_n + \dot{y}_n y_n)}{\dot{x}_n^2 + \dot{y}_n^2} \tag{11}$$

Note this is a version of τ defined as *true tau* [35], as opposed to the alternate τ definitions of *modified tau* [35] and *simplified tau* [4]. For simplicity, the n subscript is removed for the remainder of the equations.

The corresponding CPA horizontal range, r_{CPA}, is:

$$r_{CPA} = \sqrt{(x + \tau\dot{x})^2 + (y + \tau\dot{y})^2} \tag{12}$$

To get the vertical distances at the horizontal WCT entry and exit (z_+ and z_-), where $r_{CPA} = r_{MD}$, equation (12) is converted into a quadratic:

$$r_{MD}^2 = (x + \dot{x}\tau_\pm)^2 + (y + \dot{y}\tau_\pm)^2 \tag{13}$$

Solving this quadratic for $\tau_\pm$, the time to entry, τ_+, and time to exit, τ_-, are:

$$\begin{aligned} \tau_+ &= \tau - \frac{\sqrt{(x\dot{x}+y\dot{y})^2 - (\dot{x}^2+\dot{y}^2)(x^2+y^2-r_{MD}^2)}}{\dot{x}^2+\dot{y}^2} \\ \tau_- &= \tau + \frac{\sqrt{(x\dot{x}+y\dot{y})^2 - (\dot{x}^2+\dot{y}^2)(x^2+y^2-r_{MD}^2)}}{\dot{x}^2+\dot{y}^2} \end{aligned} \tag{14}$$

The vertical distances at the WCT entry and exit, z_+ and z_- are then:

$$\begin{aligned} z_+ &= z + \dot{z}\tau_+ \\ z_- &= z + \dot{z}\tau_- \end{aligned} \tag{15}$$

Hazard State Estimate Error Variances

To get *hazard state* estimate error variances, we first linearize equations (11), (12), and (15), which is described in the previous work [10]. For example, the τ transformation, $\mathbf{a}_\tau^T$, is the vector of the Taylor Series partial derivatives of τ with respect to trajectory states. The τ estimate error variance, σ_τ^2, is determined by transforming $\hat{\mathbf{P}}_x$ from equation (9):

$$\sigma_\tau^2 = \mathbf{a}_\tau^T \hat{\mathbf{P}}_x \mathbf{a}_\tau \tag{16}$$

Given zero-mean sensor measurement errors, the resulting distribution for the estimated τ is:

$$\hat{\tau} \sim N(\tau, \sigma_\tau^2) \tag{17}$$

The distributions for the estimated parameters $\hat{r}_{CPA}$, $\hat{z}_+$, and $\hat{z}_-$ are found the same way:

$$\hat{r}_{CPA} \sim N(r_{CPA}, \sigma_r^2) \tag{18}$$

$$\hat{z}_+ \sim N(z_+, \sigma_+^2) \tag{19}$$

$$\hat{z}_- \sim N(z_-, \sigma_-^2) \tag{20}$$

The hazard state estimates ($\hat{\tau}$, $\hat{r}_{CPA}$, $\hat{z}_+$, and $\hat{z}_-$) are correlated.

INTEGRITY RISK

Hazardously misleading information (HMI) occurs when a hazard exists, but that hazard is not sensed. This HMI leads the own aircraft to not maneuver when a self-separation maneuver is warranted. To ensure there is an acceptable probability of HMI, P_{HMI}, hazard thresholds (τ_{SS}, r_{MD}, and z_{MD}) are adjusted by adding multiples of the hazard state standard deviations. The self-separation integrity risk is P_{HMI}.

The probability of HMI in equation (21) reflects the probability of an imminent (at or within τ_{SS} seconds) intruder aircraft violation of the WCT.

$$P_{HMI} = P(\text{Sense No Hazard}|\text{Hazard Exists}) \tag{21}$$

Hazard Exists describes a condition where the intruder is within the horizontal time to CPA threshold on a trajectory that penetrates the WCT distance threshold cylinder. This means the following conditions are occurring simultaneously:

- The actual time to closest approach, τ, is less than or equal to τ_{SS}
- AND the actual horizontal CPA distance, r_{CPA}, is at or within r_{MD}
- AND one of the following three conditions are occurring:
  - The intruder trajectory will enter or exit the WCT cylinder from the side ($|z_+| \leq z_{MD} \ \cup \ |z_-| \leq z_{MD}$)
  - OR the intruder trajectory will descend into the WCT cylinder from the top and exit from the bottom ($z_+ > z_{MD} \ \cap \ z_- < -z_{MD}$)
  - OR the intruder trajectory will climb into the WCT cylinder from the bottom and exit from the top ($z_+ < -z_{MD} \ \cap \ z_- > z_{MD}$)

In this case, the own aircraft should initiate a self-separation maneuver.

$$\begin{gathered}\text{Hazard Exists} = \\ [\tau_n \leq \tau_{SS} \ \cap \ r_{CPA} \leq r_{MD} \ \cap \\ (\ |z_+| \leq z_{MD} \ \cup \ |z_-| \leq z_{MD} \ \cup \\ [z_+ > z_{MD} \ \cap \ z_- < -z_{MD}] \ \cup \\ [z_+ < -z_{MD} \ \cap \ z_- > z_{MD}]\ )\ ]\end{gathered} \tag{22}$$

Sense No Hazard (SNH) describes a case where any one of the following events occurs:

- The estimated time to closest approach, $\hat{\tau}$, is greater than the adjusted threshold $\tau_{SS} + k_\tau \sigma_\tau$
- OR the estimated horizontal CPA, $\hat{r}_{CPA}$, is beyond the adjusted threshold $r_{MD} + k_r \sigma_r$
- OR while the estimated horizontal CPA, $\hat{r}_{CPA}$, is at or within the adjusted threshold $r_{MD} + k_r \sigma_r$:
  - the estimated intruder trajectory will be above the adjusted WCT cylinder
  - OR the estimated intruder trajectory will be below the adjusted WCT cylinder

The standard deviation coefficient, k, is defined later in equation (25) for the τ hazard state. Any one of these misleading estimates can cause HMI that leads the own aircraft to not maneuver when a self-

separation maneuver is warranted.

$$\begin{aligned}\text{SNH} = [&\hat{\tau}_n > \tau_{SS} + k_\tau \sigma_\tau \cup \\ &\hat{r}_{CPA} > r_{MD} + k_r \sigma_r \cup \\ &[\hat{r}_{CPA} \leq r_{MD} + k_r \sigma_r \cap \\ &(\hat{z}_+ > z_{MD} + k_+ \sigma_+ \cap \\ &\hat{z}_- > z_{MD} + k_- \sigma_-)] \cup \\ &[\hat{r}_{CPA} \leq r_{MD} + k_r \sigma_r \cap \\ &(\hat{z}_+ < -z_{MD} + k_+ \sigma_+ \cap \\ &\hat{z}_- < -z_{MD} + k_- \sigma_-)] \ ]\end{aligned} \tag{23}$$

P_{HMI} must meet a predefined integrity risk requirement, I_{SS}. This can be broken down into I_{SS} allocations for each hazard state. For example, for τ:

$$P_{HMI} = Q(k_\tau) = I_\tau \tag{24}$$

where $Q(x)$ is the right tail probability of the standard normal distribution. This is used to obtain k_τ:

$$k_\tau = Q^{-1}(I_\tau) \tag{25}$$

k_r is found in a similar way, detailed in the previous work [10].

However, in the z direction, to determine k_+ and k_- is a bit more complicated. Given that the 2D horizontal intruder trajectory projection penetrates the 2D WCT circle ($r_{CPA} \leq r_{MD}$), figure 5 shows the nine different ways the 3D intruder trajectory can approach the WCT cylinder, based on the values of z_+ and z_-. In the upper-right section, the intruder passes completely above the WCT ($z_+ > z_{MD} \ \cap \ z_- > z_{MD}$). In the lower-left section, the intruder passes completely below the WCT ($z_+ < -z_{MD} \ \cap \ z_- < -z_{MD}$). In the seven other cases, the intruder penetrates the WCT, representing a WCT violation. In the middle-top, middle-middle, and middle-bottom sections, the intruder enters the WCT from the side ($|z_+| \leq z_{MD}$). In the middle-left, middle-middle, and middle-right sections, the intruder exits the WCT out of the side ($|z_-| \leq z_{MD}$). In the lower-right section, the intruder descends through the WCT, entering from the cylinder's top and exiting through the cylinder's bottom ($z_+ > z_{MD} \ \cap \ z_- < -z_{MD}$). In the upper-left section, the intruder climbs through the WCT, entering from the cylinder's bottom and exiting through the cylinder's top ($z_+ < -z_{MD} \ \cap \ z_- > z_{MD}$).

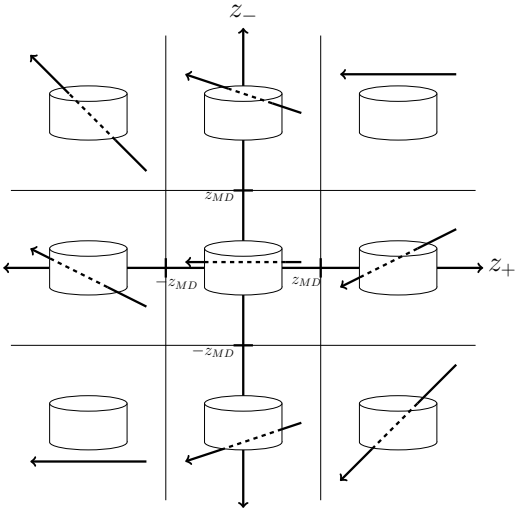

Fig. 5. Possible Intruder Trajectories in ($\hat{z}_+$; $\hat{z}_-$) Plane

Figure 6 relates the estimated ($\hat{z}_+$, $\hat{z}_-$) plane to HMI. Given that the intruder actually penetrates the WCT cylinder, HMI would mean the sensor estimated the intruder trajectory to be completely above the cylinder (upper-right shaded area) or completely below the cylinder (lower-left shaded area). In the left figure of figure 6, the unshaded areas in white represent areas where the hazard is sensed.

The values of actual z_+ and z_- that maximize P_{HMI} are somewhere on the border lines of the shaded areas of the left figure. Those borders represent either $z_+ = z_{MD} + k_+\sigma_+$, $z_+ = -z_{MD} - k_+\sigma_+$, $z_- = z_{MD} + k_-\sigma_-$, or $z_- = -z_{MD} - k_-\sigma_-$. Since for each encounter, there will only be one actual z_+ and one actual z_-, there only needs to be one worst case scenario considered to define P_{HMI} for the z direction. In the right figure of figure 6, we consider the $z_+ = z_- = z_{MD}$ scenario for illustration purposes (where the joint normal probability density ellipse is centered). This is a boundary case with an intruder trajectory at the top border of the WCT cylinder. Computing the exact HMI requires an integration of the joint ($\hat{z}_+$,

$\hat{z}_-$) probability which is computationally expensive. Instead, we use bounds on both the top and bottom HMI's. Depending on the orientation of the ellipse (which depends on the values of the ($\hat{z}_+$, $\hat{z}_-$) covariance matrix), $z_+ = z_- = z_{MD}$ may or may not be the worst case scenario. However, the following bound covers all P_{HMI} boundaries, so that the worst case scenario is covered:

$$P_{HMItop} \leq \frac{Q(k_+) + Q(k_-)}{2} \tag{26}$$

$$P_{HMIbot} \leq \frac{Q\left(k_+ + \frac{2z_{MD}}{\sigma_+}\right) + Q\left(k_- + \frac{2z_{MD}}{\sigma_-}\right)}{2} \tag{27}$$

These bounds include the excess light shaded area in the right figure of figure 6, as well as the overlapped dark shaded area, which includes the P_{HMI} we are interested in capturing. Putting them both together:

$$P_{HMIz} \leq \tfrac{1}{2}(Q(k_+) + Q(k_-) + Q\left(k_+ + \tfrac{2z_{MD}}{\sigma_+}\right) + Q\left(k_- + \tfrac{2z_{MD}}{\sigma_-}\right)) \leq I_z \tag{28}$$

Where I_z is the integrity requirement in the z direction. The k coefficients will be chosen to ensure the inequality in equation (28) is true. Note an intruder trajectory at the bottom of the WCT cylinder (with a probability density ellipse centered at ($-z_{MD}$, $-z_{MD}$)) would mirror the right figure of figure 6 and the resulting bounding would be the same as in equation (28).

Figure 7 depicts a worst case 2D HMI scenario, where the actual r_{CPA} is just within the r_{MD} but the estimate $\hat{r}_{CPA}$ is just beyond the adjusted threshold $r_{MD} + k_r\sigma_r$. The adjusted threshold ensures that this case occurs with a probability less than or equal to I_r (if we allocate I_r as an integrity requirement specifically for r_{CPA}).

To account for the correlation of hazard state estimates, the total probability of HMI is bounded by the following:

$$P_{HMI} \leq Q(k_\tau) + Q(k_r) + \tfrac{1}{2}(Q(k_+) + Q(k_-) + Q\left(k_+ + \tfrac{2z_{MD}}{\sigma_+}\right) + Q\left(k_- + \tfrac{2z_{MD}}{\sigma_-}\right)) \leq I_{SS} \tag{29}$$

This allows us to determine integrity coefficients (k_τ, k_r, k_+, k_-) based on an integrity risk requirement, I_{SS}. The previous work [10] has a more detailed explanation of the derivation of this methodology.

CONTINUITY RISK

A false alert (FA) occurs when no hazard exists, but a hazard is falsely sensed. This FA leads the own aircraft to maneuver when a self-separation maneuver is not warranted. To ensure there is an acceptable P_{FA}, continuity buffers are added to the integrity-adjusted distance thresholds. The alert to maneuver will still be based on the integrity-adjusted distance thresholds. The area inside each continuity buffer is where false alerts can occur with a probability higher than a given continuity requirement. The self-separation continuity risk is P_{FA}.

The probability of FA in equation (30) reflects the probability when no hazard exists, but a hazard is falsely sensed.

$$P_{FA} = P(\text{Sense Hazard}|\text{No Hazard Exists}) \tag{30}$$

No Hazard Exists describes a condition where the intruder trajectory is outside the WCT distance threshold cylinder. This means any of the following conditions occur:

- The actual time to closest approach, τ, is greater than the threshold τ_{SS}
- OR the actual horizontal CPA, r_{CPA}, is beyond the threshold r_{MD}
- OR while the actual horizontal CPA, r_{CPA}, is at or within the threshold r_{MD}:
  - the actual intruder trajectory is above the WCT cylinder
  - OR the actual intruder trajectory is below the WCT cylinder

$$\begin{aligned}&\text{No Hazard Exists} = \\ &[\tau_n > \tau_{SS} \ \cup \ r_{CPA} > r_{MD} \\ &\cup [r_{CPA} \leq r_{MD} \\ &\cap (z_+ > z_{MD} \ \cap \ z_- > z_{MD})] \\ &\cup [r_{CPA} \leq r_{MD} \\ &\cap (z_+ < -z_{MD} \ \cap \ z_- < -z_{MD})] \ ]\end{aligned} \tag{31}$$

Sense Hazard describes a case with the following conditions:

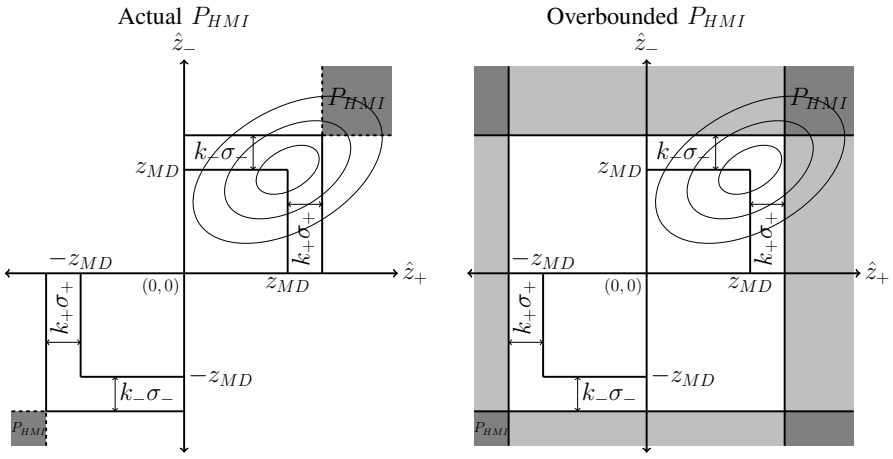

Fig. 6. Integrity Risk Correlation Between $\hat{z}_+$ and $\hat{z}_-$

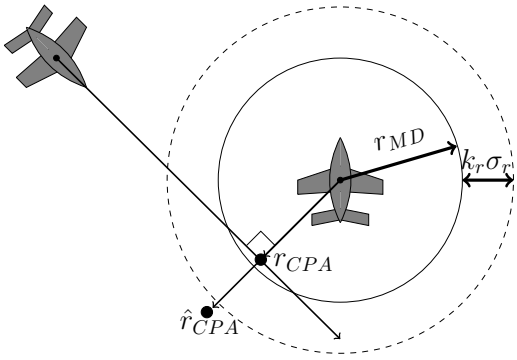

Fig. 7. Worst Case HMI Scenario for r_{CPA}

- The estimated time to closest approach, $\hat{\tau}$, is less than or equal to the adjusted threshold, $\tau_{SS} + k_\tau\sigma_\tau$
- AND the estimated horizontal CPA distance, $\hat{r}_{CPA}$, is at or within the adjusted threshold, $r_{MD} + k_r\sigma_r$
- AND one of the following three conditions is occurring:
  - The estimated intruder trajectory will enter or exit the adjusted WCT cylinder from the side ($|\hat{z}_+| \leq z_{MD} + k_+\sigma_+ \ \cup \ |\hat{z}_-| \leq z_{MD} + k_-\sigma_-$)
  - OR the estimated intruder trajectory will descend into the adjusted WCT cylinder from the top and exit from the bottom ($\hat{z}_+ > z_{MD} + k_+\sigma_+ \ \cap \ \hat{z}_- < -z_{MD} - k_-\sigma_-$)
  - OR the estimated intruder trajectory will climb into the adjusted WCT cylinder from the bottom and exit from the top ($\hat{z}_+ < -z_{MD} - k_+\sigma_+ \ \cap \ \hat{z}_- > z_{MD} + k_-\sigma_-$)

The own aircraft senses the need to initiate a self-separation maneuver when an actual hazard does not exist.

$$\begin{aligned}&\text{Sense Hazard} = \\ &[\hat{\tau}_n \leq \tau_{SS} + k_\tau\sigma_\tau \ \cap \ \hat{r}_{CPA} \leq r_{MD} + k_r\sigma_r \\ &\cap \ (\ |\hat{z}_+| \leq z_{MD} + k_+\sigma_+ \\ &\cup \ \ |\hat{z}_-| \leq z_{MD} + k_-\sigma_- \\ &\cup [\hat{z}_+ > z_{MD} + k_+\sigma_+ \\ &\cap \ \ \hat{z}_- < -z_{MD} - k_-\sigma_-] \\ &\cup [\hat{z}_+ < -z_{MD} - k_+\sigma_+ \\ &\cap \ \ \hat{z}_- > z_{MD} + k_-\sigma_-])]\end{aligned} \tag{32}$$

Here, P_{FA} must meet a predefined continuity risk requirement, C_{SS}. This can be broken down into each hazard state. For example, for τ:

$$P_{FA} = \Phi(-\ell_\tau) = C_\tau \tag{33}$$

where $\Phi(x)$ is the cumulative distribution function.

This is used to obtain ℓ_τ:

$$\ell_\tau = -\Phi^{-1}(C_\tau) \tag{34}$$

ℓ_r is found in a similar way detailed in the previous work [10]. When τ is between $\tau_{SS} + k_\tau\sigma_\tau$ and $\tau_{SS} + (k_\tau + \ell_\tau)\sigma_\tau$, the own aircraft may FA with a probability higher than the continuity requirement. This means that the lower limit on protectable τ is $\tau_{SS} + (k_\tau + \ell_\tau)\sigma_\tau$. We will henceforth call this the *protection level*.

To determine ℓ_+ and ℓ_-, we refer to the ($\hat{z}_+$, $\hat{z}_-$) planes in figure 8. In the left plane of figure 8, the shaded area reflects the P_{FA} region for the intruder trajectory at the top of the WCT cylinder. In the right plane of figure 8, the P_{FA} region is over-bounded by the shaded area, with the overlapped dark shaded area counted twice. For a continuity requirement in the z direction, C_z, the resulting bound becomes:

$$P_{FAz} \leq \Phi(-\ell_+) + \Phi(-\ell_-) \leq C_z \tag{35}$$

Figure 9 depicts a worst case FA scenario, where the actual r_{CPA} is just beyond the protection level $r_{MD} + k_r\sigma_r + \ell_r\sigma_r$ while the estimate $\hat{r}_{CPA}$ is just within the integrity-adjusted threshold $r_{MD} + k_r\sigma_r$. The continuity buffer ensures this case occurs with a probability less than or equal to C_r (if we allocate C_r as a continuity requirement specifically for r_{CPA}).

The total probability of FA is bounded by the following:

$$\begin{aligned} P_{FA} \leq \tfrac{\Phi(-\ell_\tau)+\Phi(-\ell_r)}{2} \\ +\Phi(-\ell_+) + \Phi(-\ell_-) \leq C_{SS} \end{aligned} \tag{36}$$

This allows us to select continuity coefficients (ℓ_τ, ℓ_r, ℓ_+, ℓ_-) based on a continuity risk requirement, C_{SS}. Again, the previous work [10] has a more detailed explanation of the derivation of this methodology.

RELATING INTEGRITY AND CONTINUITY TO SENSOR REQUIREMENTS

With a predefined integrity risk requirement, I_{SS}, and a predefined continuity requirement, C_{SS}, the SAA system will alert and maneuver depending on how large each hazard state standard deviation (σ_τ, σ_r, σ_+, and σ_-) is at each sampled time. As the SAA system gets more intruder measurements, each hazard state standard deviation will get smaller over time. Each hazard state's protection level must be reasonably close to the original WCT before a hazard test can be executed. Otherwise, the resulting protected separation distances can be very large, leading to ATC capacity issues. To mitigate this, a certification authority will need to determine an acceptable fractional margin, ϵ, on all three original hazard thresholds (τ_{SS}, r_{MD}, and z_{MD}) for $(k + \ell)\sigma$. This is expressed mathematically as:

$$\begin{aligned} \epsilon_\tau &= \tfrac{(k_\tau+\ell_\tau)\sigma_\tau}{\tau_{SS}} \\ \epsilon_r &= \tfrac{(k_r+\ell_r)\sigma_r}{r_{MD}} \\ \epsilon_z &= \tfrac{(k_+ +\ell_+)\sigma_+}{z_{MD}} = \tfrac{(k_- +\ell_-)\sigma_-}{z_{MD}} \end{aligned} \tag{37}$$

Obviously, it is desirable that ϵ is small. However, achieving $\epsilon = 0$ is impossible because it would require perfect sensors such that $\sigma_\tau = \sigma_r = \sigma_+ = \sigma_- = 0$. The fractional margin, ϵ, can then be used to define practical operational limits on hazard state standard deviations, $\tilde{\sigma}$'s. The hazard state standard deviation operational limits are:

$$\begin{aligned} \tilde{\sigma}_\tau \triangleq \tfrac{\epsilon\tau_{SS}}{k_\tau+\ell_\tau}, \quad \tilde{\sigma}_r \triangleq \tfrac{\epsilon r_{MD}}{k_r+\ell_r}, \\ \tilde{\sigma}_+ \triangleq \tfrac{\epsilon z_{MD}}{k_+ +\ell_+}, \quad \tilde{\sigma}_- \triangleq \tfrac{\epsilon z_{MD}}{k_- +\ell_-} \end{aligned} \tag{38}$$

At the aircraft, the SAA hazard detection test described in equation (21) can be carried out with required integrity and continuity when all hazard state σ's decrease below their respective operational limits ($\tilde{\sigma}$'s).

While the intruder aircraft approaches the own aircraft, the hazard state standard deviations will decrease as the number of accumulated sensor measurements increases. Nevertheless, not all sensors or sensor-suites are capable of ensuring that the hazard state standard deviations can reduce below their operational limits in time to perform a hazard detection test (with required integrity and continuity) before a hazard actually occurs. To identify sensors that can meet this requirement, operational limits on hazard states are set as follows:

$$\begin{aligned} \tilde{\tau}_\tau &\triangleq (1+\epsilon)\tau_{SS} \\ \tilde{r} &\triangleq (1+\epsilon)r_{MD} \\ \tilde{z} &\triangleq (1+\epsilon)z_{MD} \end{aligned} \tag{39}$$

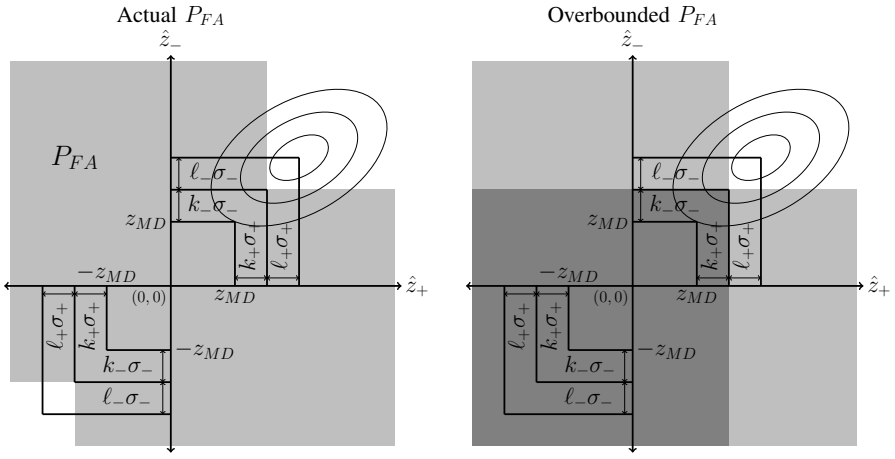

Fig. 8. Continuity Risk Correlation Between $\hat{z}_+$ and $\hat{z}_-$

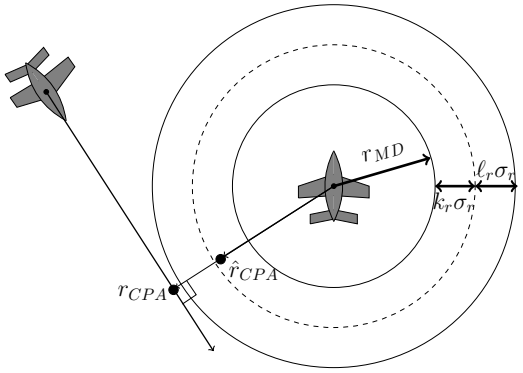

Fig. 9. Worst Case FA Scenario for r_{CPA}

The WCT distance threshold operational limits ($\tilde{r}$ and $\tilde{z}$) can be translated to operational limits on τ because there is an associated time when these limits are reached. Using the intruder's estimated projected trajectory, we can determine the τ's when r and z are estimated to cross their respective operational limits ($\tilde{r}$, $\tilde{z}$). $\tilde{\tau}$ is the maximum of each of the three hazard threshold $\tilde{\tau}$'s:

$$\tilde{\tau} = \max(\tilde{\tau}_\tau, \tilde{\tau}_r, \tilde{\tau}_z) \tag{40}$$

For realistic WCT thresholds and aircraft velocities, $\tilde{\tau}_r$ and $\tilde{\tau}_z$ will typically be much lower than $\tilde{\tau}_\tau$. $\tilde{\tau}$ will usually be determined by $\tilde{\tau}_\tau$. However, for low relative aircraft velocities, $\tilde{\tau}_r$ and $\tilde{\tau}_z$ will need to be considered.

Figure 10 depicts how the operational limit relates to sensor requirements. The plots represent two different sensors. For a sensor to meet requirements, each of its σ curves, for each of its hazard states, must be less than its $\tilde{\sigma}$ at a τ greater than $\tilde{\tau}$. In the plots, each curve is non-dimensionalized by its $\tilde{\sigma}$, resulting in a common y-axis where the required threshold is one. If a sensor $\sigma/\tilde{\sigma}$ curve crosses 1 at a τ less than $\tilde{\tau}$, it will cross into the gray shaded area, which indicates a sensor that will FA at a probability higher than the continuity risk requirement and potentially violate integrity at a probability higher than the integrity risk requirement. In the figure, only Sensor A meets the integrity and continuity risk requirements.

In order to apply this methodology, a sensor must have characteristics (sensor uncertainty, sensor range, and sample interval) to reduce each hazard state σ-value below each $\tilde{\sigma}$ (or its non-dimensionalized $\sigma/\tilde{\sigma}$-value below 1) prior to its $\tilde{\tau}$, as depicted in Figure 10. If a given sensor is not good enough, sensor measurement uncertainty must be reduced, sensor range must be extended, and/or sample rate must be increased. During operation, once all hazard state σ's are reduced below their corresponding $\tilde{\sigma}$'s, there only needs to be one test.

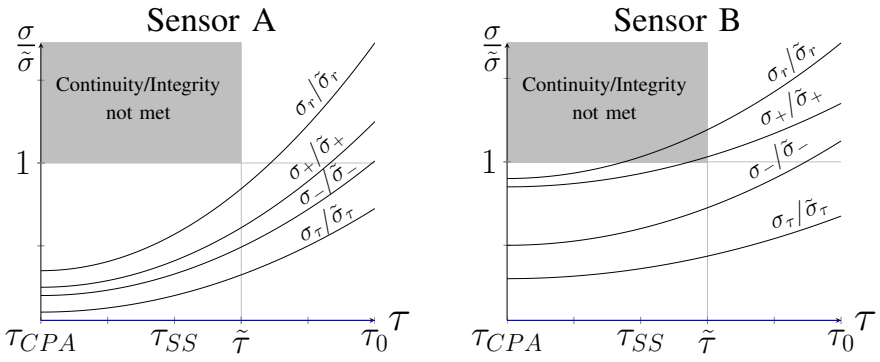

Fig. 10. Applying Operational Limits to Sensor Requirements

From there, an alerted UAS can maneuver based on timing: when $\hat{\tau} < \tilde{\tau}$.

SENSITIVITY ANALYSIS

This sensitivity analysis assumes a constant relative intruder velocity and addresses three dimensional intruder trajectories.

In [36], typical radar SAA sensors are described as having an azimuth and elevation accuracy of 0.5° to 2°, a range accuracy of 10 ft to 200 feet, an update rate of 0.2 Hz to 5 Hz, and a detection range of 5 nautical miles (NM) to 10 NM. In [26] and [37], a nominal radar SAA sensor is described as having a range standard deviation (σ_ρ) of 24.6 feet, an azimuth standard deviation (σ_θ) of 0.24°, an elevation standard deviation (σ_ϕ) of 0.72°, and detection range of 8 NM. Also, in [36], typical EO SAA sensors are described as having an azimuth and elevation accuracy of 0.1° to 0.5°, an update rate of 20 Hz, and a detection range of 2 NM to 5 NM. As a result we use a composite nominal sensor having a σ_ρ of 5 feet, a σ_θ of 0.05°, a σ_ϕ of 0.05°, a detection range of 8 NM, and an update rate of 5 Hz.

For τ and r_{MD}, the WCT established by the RTCA SC-228 SARP is used: τ_{SS} of 35 seconds and an r_{MD} of 4000 feet [9]. Corresponding ϵ_τ and ϵ_r of 10% are chosen leading to $\tilde{\tau}$ of 38.5 seconds and $\tilde{r}$ of 4400 feet. For z_{MD}, 450 feet is chosen, denoting the 500 foot difference between VFR and IFR altitudes [38], [39]. The vertical WCT established by the SC-228 SARP is selected to be $\tilde{z} = 700$ feet [9], leading to $\epsilon_z = 56\%$. The desired integrity requirement, $I_{SS} = 10^{-6}$, and the continuity requirement, $C_{SS} = 10^{-3}$, are based on the FAA's definition of major and minor failure conditions [40]. For simplicity, the integrity and continuity risk coefficients are set to be equal: $k_\tau = k_r = k_+ = k_- = 4.98$ and $\ell_\tau = \ell_r = \ell_+ = \ell_- = 3.4$.

Intruder Trajectories

The intruder trajectories analyzed are based on the intruder being initially observed directly in front of the own aircraft at the sensor range of 8 NM. In the x-y plane, the trajectories are based on the worst-case 2D trajectories analyzed in the previous work [10], which were head-on and tangent to the r_{MD} circle. These 2D trajectories are depicted in the right side of figure 11.

In the z direction, the intruder trajectory will either climb, descend, or remain level at the top (or equivalently at the bottom) of the WCT cylinder. A worst-case relative velocity of 500 knots is chosen, reflecting the closure of two aircraft at a maximum airspeed of 250 knots each. Aircraft are restricted to 250 knots below 10,000 feet per 14 CFR 91.117 [41]. The maximum relative descent rate of the intruder is based on the maximum descent rate of a likely intruder in the NAS plus the maximum climb rate of a high performing UAS. For the likely intruder, according to Appendix A of Change

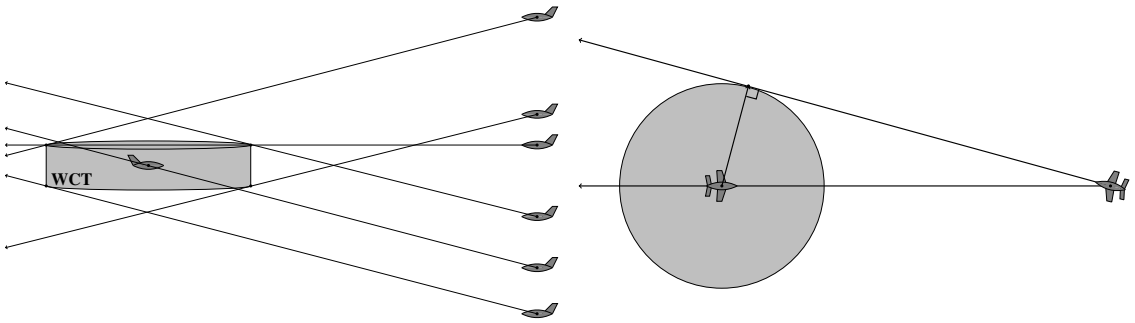

Fig. 11. Head-on Trajectories and 2D Trajectories

3 to FAA JO 7110.65V, the maximum descent for a non-fighter, fixed-wing aircraft is the Boeing 727 with a maximum descent of 4500 feet per minute (fpm) [42]. According to data synthesized in [43], the Global Hawk high-altitude long-endurance (HALE) UAV has an initial climb rate of 4000 fpm at sea level, below 200 knots. This climb rate decreases incrementally with altitude as its climb airspeed incrementally increases. Based on this, we will conservatively assume a maximum climbing airspeed for the own aircraft of approximately 3500 fpm. This leads to the assumed worst case relative intruder descending vertical velocity of 8000 fpm.

The maximum relative climb rate of the intruder is found in a similar way. For the intruder, according to Appendix A of Change 3 to FAA JO 7110.65V, the maximum climb for a non-fighter, fixed-wing aircraft is the Boeing 737-400 with a maximum climb of 6500 feet per minute (fpm) [42]. According to data synthesized in [43], the Global Hawk max descent rate is 4000 fpm. This leads to the assumed worst case relative intruder climbing vertical velocity of 10,500 fpm.

From there, we chose eleven constant-velocity 3D intruder trajectories:

- Head-on, direct collision course climbing.
- Head-on, level at z_{MD} ($z_+ = z_- = z_{MD}$).
- Tangent to the r_{MD} circle, level at z_{MD} ($z_+ = z_- = z_{MD}$).
- Head-on, descending, intercepting the top WCT border at the back ($z_- = z_{MD}$).
- Head-on, climbing, intercepting the top WCT border (z_{MD}) at the front ($z_+ = z_{MD}$).
- Tangent to the r_{MD} circle, descending, intercepting the top WCT border ($z_+ = z_- = z_{MD}$).
- Tangent to the r_{MD} circle, climbing, intercepting the top WCT border ($z_+ = z_- = z_{MD}$).
- Head-on, descending, intercepting the bottom WCT border at the front ($z_+ = -z_{MD}$).
- Head-on, climbing, intercepting the bottom WCT border at the back ($z_- = -z_{MD}$).
- Tangent to the r_{MD} circle, descending, intercepting the bottom WCT border ($z_+ = z_- = -z_{MD}$).
- Tangent to the r_{MD} circle, climbing, intercepting the bottom WCT border ($z_+ = z_- = -z_{MD}$).

The six head-on trajectories are depicted in the left side of figure 11.

Results

For the nominal sensor, all eleven trajectories met requirements (by staying out of the upper-left hand quadrant) in the σ_τ vs τ and the σ_r vs τ graphs, as depicted in figure 12 and figure 13. However, the sensor did not meet requirements (by penetrating the upper-left hand quadrant) in both vertical directions: σ_+ vs τ and σ_- vs τ, as depicted in figure 14 and figure 15. Although most of the trajectories were close to meeting requirements, for both vertical directions, there were four trajectories that were way off: both tangent climbing trajectories (depicted as green dashed lines) and, slightly better,

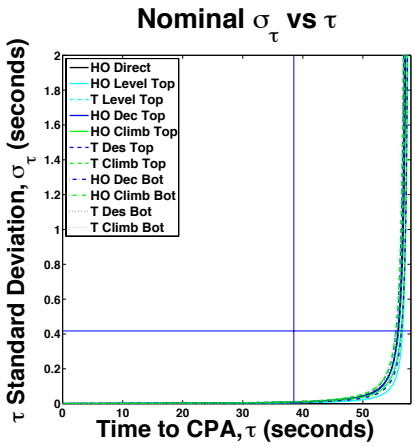

Fig. 12. Nominal Sensor σ_τ vs τ

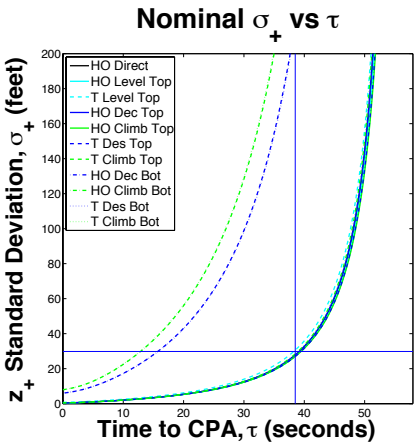

Fig. 14. Nominal Sensor σ_+ vs τ

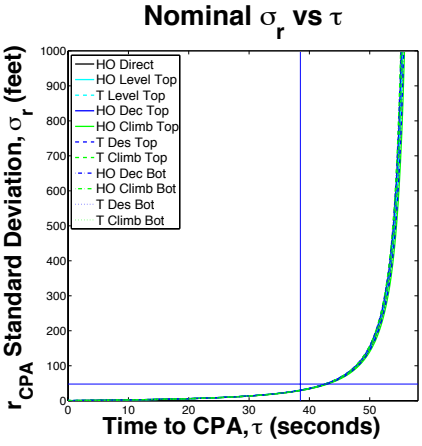

Fig. 13. Nominal Sensor σ_r vs τ

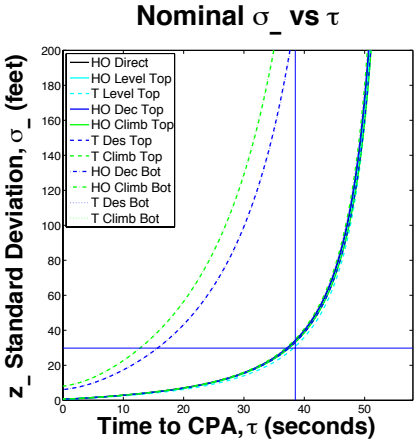

Fig. 15. Nominal Sensor σ_- vs τ

both tangent descending trajectories (depicted as blue dashed lines). Reducing the climb and descent rates of these trajectories brings their respective σ_+ vs τ and σ_- vs τ curves to meet the other seven trajectories.

To meet integrity and continuity requirements, we needed to make three adjustments. σ_+ and σ_- were most sensitive to azimuth uncertainty and we improved σ_θ by a factor of 10. Also, we increased the update rate to 8 Hz and improved σ_ϕ slightly to 0.03°. These results are depicted in figure 16 and figure 17. Although our adjustments to update rate, azimuth uncertainty, and elevation uncertainty resulted in the desired outcome, there are other adjustments that could have been made to improve sensor performance. For example, increasing the sensor range beyond 8 NM would allow for more measurements prior to $\tilde{\tau}$. Also, increasing each threshold's ϵ would increase its $\tilde{\sigma}$ (at the risk of decreasing airspace capacity). In addition, reallo-

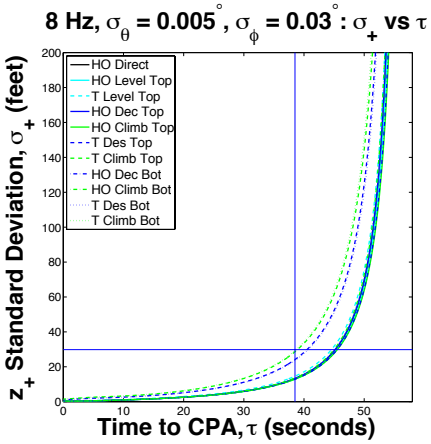

Fig. 16. Adjusted Sensor σ_+ vs τ

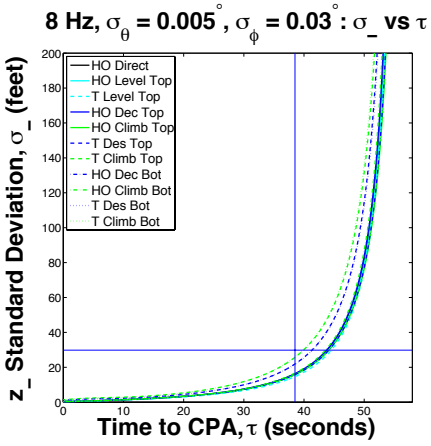

Fig. 17. Adjusted Sensor σ_- vs τ

cating k's and ℓ's unevenly among each hazard state can slightly increase $\tilde{\sigma}$ for more restrictive hazard states (such as z_+ and z_-) while decreasing $\tilde{\sigma}$ for hazard states with more margin (such as τ and r_{CPA}). Finally, reevaluating the assumptions that led to the 10,500 fpm climb rate, 8000 fpm descent rate, and 500 knot relative velocity would also impact performance.

CONCLUSIONS

In this paper, we determined integrity and continuity risk for intruder trajectories in three dimensions. A sensitivity analysis was presented to explore the sensor requirement trade space and analyze eleven restrictive 3D trajectories. The tangent climbing and descending trajectories were most restrictive. We were able adjust sensor characteristics in the analysis to meet integrity and continuity requirements. Our methodology can be used by a certification authority to certify potential SAA sensors.

ACKNOWLEDGMENTS

We would like to express our appreciation to Phil Maloney, UAS Certification Obstacle Team Leader, of the FAA Hughes Technical Center, for supporting this research, which was awarded FAA Grant #14-G-018. However, the views expressed in this paper are the authors' alone and do not necessarily represent the opinions of any other organization or person.

References

[1] Federal Aviation Administration, "Integration of Civil Unmanned Aircraft Systems (UAS) in the National Airspace System (NAS) Roadmap," Nov 2013.

[2] US House of Representatives, "FAA Modernization and Reform Act of 2012," Feb 2012.

[3] Federal Aviation Administration TCAS Program Office, "Concept of Use for the Airborne Collision Avoidance System X_U," Feb 2013.

[4] Federal Aviation Administration, "Sense and Avoid (SAA) for Unmanned Aircraft Systems (UAS), SAA Workshop Second Caucus Report," Jan 2013.

[5] Anderson, E. E., Watson, W., Johnson, K., Kimber, N. R., and Weiss, N. J., "A Legal Analysis of 14 C.F.R. Part 91 See and Avoid Rules to Identify Provisions Focused on Pilot Responsibilities to See and Avoid in the National Airspace System." Tech. rep., University of North Dakota-U.S. Department of Transportation, Federal Aviation Administration, Dec 2013.

[6] 14 CFR 91.113, "Right-of-way Rules: Except Water Operations," Jul 2004.

[7] Weibel, R. E., Edwards, M. W. M., and Fernandes, C. S., "Establishing a Risk-Based Separation Standard for Unmanned Aircraft Self Separation," *Ninth USA/Europe Air Traffic Management Research and Development Seminar*, Berlin, Germany, Jun 2011.

[8] Lee, S. M., Park, C., Johnson, M. A., and Mueller, E. R., "Investigating Effects of Well Clear Definitions on UAS Sense-And-Avoid Operations," *AIAA Aviation Technology, Integration, and Operations Conference*, Los Angeles, CA, Apr 2013.

[9] Cook, S. P., Brooks, D., Cole, R., Hackenberg, D., and Raska, V., "Defining Well Clear for Unmanned Aircraft Systems," *AIAA SciTech*, Kissimmee, FL, Jan 2015.

[10] Jamoom, M. B., Joerger, M., and Pervan, B., "Unmanned Aircraft System Sense and Avoid Integrity and Continuity Risk for Non-Cooperatve Intruders," *AIAA SciTech*, Kissimmee, FL, Jan 2015.

[11] Kuchar, J. K. and Yang, L. C., "A Review of Conflict Detection and Resolution Modeling Methods," *IEEE Transactions on Intelligent Transportation Systems*, Vol. 1, No. 4, Dec 2000, pp. 179–189.

[12] Drumm, A., Andrews, J., Hall, T., Heinz, V., Kuchar, J., Thompson, S., and Welch, J., "Remotely Piloted Vehicles in Civil Airspace: Requirements and Analysis Methods for the Traffic Alert and Collision Avoidance System (TCAS) and See-And-Avoid Systems," *IEEE Digital Avionics Systems Conference*, Vol. 2, Oct 2004, pp. 12.D.1–1–14.

[13] Dalamagkidis, K., Valavanis, K., and Piegl, L., "On unmanned aircraft systems issues, challenges and operational restrictions preventing integration into the National Airspace System," *Progress in Aerospace Sciences*, Vol. 44, No. 7, Jul 2008, pp. 503–519.

[14] Prats, X., Delgado, L., Ramirez, J., Royo, P., and Pastor, E., "Requirements, Issues, and Challenges for Sense and Avoid in Unmanned Aircraft Systems," *AIAA Journal of Aircraft*, Vol. 49, No. 3, May 2012, pp. 677–687.

[15] Yu, X. and Zhang, Y., "Sense and avoid technologies with applications to unmanned aircraft systems: Review and prospects," *Progress in Aerospace Sciences*, Vol. 74, Apr 2015, pp. 152–166.

[16] McLaughlin, M. P. and Zeitlin, A. D., "Safety Study of TCAS II for Logic Version 6.04," Tech. rep., MITRE Corporation-U.S. Department of Transportation, Federal Aviation Administration, Jul 1992.

[17] Espindle, L., Griffith, J., and Kuchar, J., "Safety Analysis of Upgrading to TCAS Version 7.1 Using the 2008 U.S. Correlated Encounter Model." Tech. rep., Lincoln Laboratory, Massachusetts Institute of Technology, May 2009.

[18] ICAO 9689-AN/953, "Manual on Airspace Planning Methodology for the Determination of Separation Minima," Dec 1998.

[19] Kim, J.-H., Lee, D. W., Cho, K.-R., Jo, S.-Y., Kim, J.-H., Min, C.-O., Han, D.-I., and Cho, S.-J., "Development of an electro-optical system for small UAV," *Aerospace Science and Technology*, Vol. 14, No. 7, Oct 2010, pp. 505–511.

[20] Kochenderfer, M. J., Edwards, M. W. M., Espindle, L. P., Kuchar, J. K., and Griffith, J. D., "Airspace Encounter Models for Estimating Collision Risk," *AIAA Journal of Guidance, Control, and Dynamics*, Vol. 33, No. 2, Mar 2010, pp. 487–499.

[21] Chryssanthacopoulos, J. P. and Kochenderfer, M. J., "Accounting for State Uncertainty in Collision Avoidance," *AIAA Journal of Guidance, Control, and Dynamics*, Vol. 34, No. 4, Jul 2011, pp. 951–960.

[22] Billingsley, T. B., Kochenderfer, M. J., and Chryssanthacopoulos, J. P., "Collision Avoidance for General Aviation," *IEEE Aerospace and Electronic Systems Magazine*, Vol. 27, No. 7, Jul 2012, pp. 4–12.

[23] Heisey, C. W., Hendrickson, A. G., Chludzinski, B. J., Cole, R. E., Ford, M., Herbek, L., Ljungberg, M., Magdum, Z., Marquis, D., Mezhirov, A., Pennell, J. L., Roe, T. A., and Weinert, A. J., "A Reference Software Architecture to Support Unmanned Aircraft Integration in the National Airspace System," *Journal of Intelligent & Robotic Systems*, Vol. 69, No. 1-4, Jan 2013, pp. 41–55.

[24] Lee, H.-T., Meyn, L. A., and Kim, S., "Probabilistic Safety Assessment of Unmanned Aerial System Operations," *AIAA Journal of Guidance, Control, and Dynamics*, Vol. 36, No. 2, Mar 2013, pp. 610–616.

[25] Owen, M. P., Duffy, S. M., and Edwards, M. W. M., "Unmanned Aircraft Sense and Avoid Radar: Surrogate Flight Testing Performance Evaluation," *IEEE Radar Conference*, Cincinnati, OH, May 2014, pp. 548–551.

[26] Edwards, M. W. M. and Owen, M. P., "Validating a Concept for Airborne Sense and Avoid," *American Control Conference*, Portland, OR, Jun 2014, pp. 1192–1197.

[27] ICAO, "International Standards and Recommended Practices," July 2006.

[28] RTCA SC-159, "Minimum Aviation System Performance Standards for the Local Area Augmentation System," 2004.

[29] Kelly, R. J. and Davis, J. M., "Required Navigation Performance (RNP) for Precision Approach and Landing with GNSS Application," *Navigation, Journal of the Institute of Navigation*, Vol. 41, No. 1, Spring 1994, pp. 1–30.

[30] Pullen, S., "What are the Differences Between Accuracy, Integrity, Continuity, and Availability, and How are they Computed?" *InsideGNSS*, Sep-Oct 2008, pp. 20–24.

[31] DeCleene, B., "Defining Pseudorange Integrity - Overbounding," *Institute of Navigation GPS Conference*, Salt Lake City, UT, Sep 2000, pp. 1916–1924.

[32] Rife, J., Pullen, S., Enge, P., and Pervan, B., "Paired Overbounding for Non-ideal LAAS and WAAS Error Distributions," *IEEE Transactions on Aerospace and Electronic Systems*, Vol. 42, No. 4, Oct 2006, pp. 1386–1395.

[33] Gelb, A., editor, *Applied Optimal Estimation*, The MIT Press, sixteenth ed., 2001.

[34] Bryson, A. E., *Applied Linear Optimal Control*, Cambridge University Press, 2002.

[35] RTCA SC-147, "Minimum Operational Performance Standards for Traffic Alert and Collision Avoidance System II," 2008.

[36] Chen, R. H., Gevorkian, A., Fung, A., Chen, W.-Z., and Raska, V., "Multi-Sensor Data Integration for Autonomous Sense and Avoid," *AIAA Infotech@Aerospace*, St Louis, MO, Mar 2011.

[37] Edwards, M., "A Safety Driven Approach to the Development of an Airborne Sense and Avoid System," *AIAA Infotech@Aerospace*, Garden Grove, CA, Jun 2012.

[38] 14 CFR 91.159, "VFR cruising altitude or flight level," Dec 2003.

[39] 14 CFR 91.179, "IFR cruising altitude or flight level," Jun 2007.

[40] Federal Aviation Administration, "Advisory Circular 25.1309-1A - System Design and Analysis," Jun 1988.

[41] 14 CFR 91.117, "Aircraft Speed," Aug 1993.

[42] Federal Aviation Administration, "JO 7110.65V, Change 3, Air Traffic Organization Policy," Jun 2015.

[43] Billingsley, T. B., *Safety Analysis of TCAS on Global Hawk using Airspace Encounter Models*, Master's thesis, Massachusetts Institute of Technology, Jun 2006.